TẠP CHÍ KHOA HỌC & CÔNG NGHỆ ĐẠI HỌC DUY TÂN
DTU Journal of Science and Technology 02(45) (2021) 94-102

TRƯỜNG ĐẠI HỌC DUY TÂN
DUYTAN UNIVERSITY

Effect of drying on magnetic properties of $Ba_{1-x}La_xFe_{12}O_{19}$/polyaniline composites

Ảnh hưởng của việc sấy lên từ tính của vật liệu composite $Ba_{1-x}La_xFe_{12}O_{19}$/polyaniline

Tran Ngo[a,c*], Tran Nguyen Tien[b,c]
Trần Ngọ[a,c*], Trần Nguyên Tiến[b,c]

[a]*Center for Materials Science, Institute of Research and Development, Duy Tan University, Da Nang 550000, Vietnam*
[a]*Trung tâm Khoa học Vật liệu, Viện Nghiên cứu và Phát triển Công nghệ Cao, Đại học Duy Tân, Đà Nẵng*
[b]*Center for Advanced Chemistry, Institute of Research and Development, Duy Tan University, Da Nang, 550000, Vietnam*
[b]*Trung tâm Hóa học Tiên tiến, Viện Nghiên cứu và Phát triển Công nghệ Cao, Đại học Duy Tân, Đà Nẵng*
[c]*Faculty of Natural Sciences, Duy Tan University, Da Nang, 550000, Vietnam*
[c]*Khoa Khoa học Tự nhiên, Đại học Duy Tân, Đà Nẵng*

(Ngày nhận bài: 17/03/2021, ngày phản biện xong: 24/03/2021, ngày chấp nhận đăng: 29/03/2021)

Abstract

Composites of $Ba_{1-x}La_xFe_{12}O_{19}$/polyaniline were successfully prepared. By using X-ray diffractometer, the secondary phase of α-Fe_2O_3 was detected besides the main phase of $Ba_{1-x}La_xFe_{12}O_{19}$. Phase percentage of α-Fe_2O_3 increased with the increase of La doping concentration. Lattice parameters, *a* and *c*, of the main phase were decreased with respect to the increase of the La doping concentration, *x*. The decrease of *a* and *c* could be attributed to the substitution of small ionic of La^{3+} to the larger one of Ba^{2+}. The effects of drying on magnetic properties of $Ba_{1-x}La_xFe_{12}O_{19}$/polyaniline composites were studied in two cases: un-dried and dried composites. All the magnetic parameters such as saturation magnetization, remanent magnetization, coercivity, magnetocrystalline anisotropy, magnetocrystalline anisotropy constant, and magnetocrystalline anisotropy field of the dried composites were lower than the undried ones. This change would affect the microwave absorbing properties of the composites.

Keywords: Hexaferrite; polyaniline; composite; magnetic properties.

Tóm tắt

Chúng tôi đã chế tạo thành công vật liệu composite của $Ba_{1-x}La_xFe_{12}O_{19}$/polyaniline và tiến hành khảo sát cấu trúc bằng máy tán xạ phổ tia X. Bên cạnh pha chính của $Ba_{1-x}La_xFe_{12}O_{19}$, phổ tán xạ tia X còn ghi nhận sự xuất hiện của pha phụ α-Fe_2O_3. Tỉ lệ phần trăm của pha phụ α-Fe_2O_3 tăng khi nồng độ pha tạp La tăng lên. Các thông số mạng *a* và *c* của pha chính giảm khi nồng độ La tăng lên. Điều này có thể là do sự thay thế của một ion có bán kính nhỏ (La^{3+}) cho một ion có bán kính hơn (Ba^{2+}). Ảnh hưởng của việc sấy lên tính chất từ của vật liệu composite cũng đã được khảo sát. Để tiến hành khảo sát này, vật liệu composite ban đầu được chia thành hai lô: lô 1 được giữ nguyên sau khi chế tạo (gọi là "*không sấy*") và lô 2 được đem đi nung ở 170°C (gọi là "*sấy*"). Thông số từ thu được từ hai lô composite thể hiện sự khác nhau lớn. Tất cả các giá trị của từ độ bão hòa, từ dư, lực kháng từ, tính dị hướng từ, hằng số dị hướng từ và trường

[*]*Corresponding Author:* Tran Ngo; Center for Materials Science, Institute of Research and Development, Duy Tan University, Da Nang 550000, Vietnam; Faculty of Natural Sciences, Duy Tan University, Da Nang, 550000, Vietnam.
Email: tranngo@duytan.edu.vn

dị hướng từ của "*sấy*" composite luôn thấp hơn "*không sấy*" composite. Sự thay đổi về từ tính này sẽ có ảnh hưởng đến tính chất hấp thụ sóng viba của composite.

Từ khóa: Hexaferrite; polyaniline; composite; tính chất từ.

1. Introduction

Barium M-type hexaferrite ($BaFe_{12}O_{19}$, BaM) and strontium M-type hexaferrite ($SrFe_{12}O_{19}$, SrM) belong to the hexaferrite family which includes six types: M-, W-, Y-, Z, U-, and X-types. M-type hexaferrite has simplest formula and could be described as $BaO/SrO + 6{\cdot}Fe_2O_3$. BaM is an important hard magnetic material based on its excellent characteristics such as: uniaxial magnetocrystalline anisotropy, high permeability, high saturation magnetization (M_s), high coercivity (H_c), and good chemical stability [1]. BaM is also a promising material for microwave absorbing due to a magnetic loss which is mainly produced by a natural resonance [2]. However, there are some disadvantages that could limit the microwave absorbing applications of BaM such as low dielectric constant [3], large magnetocrystalline anisotropy field, H_a = 17 kOe, and high ferromagnetic resonance frequency, f_r = 47.6 GHz [4].

In order to improve the application capability, researchers have been attempting to improve dielectric loss and reduce ferromagnetic resonance frequency. There were several approaches that have been studied such as combining BaM with other soft magnetic materials [5-7], preparing compound of BaM with high dielectric constant materials (carbon [8], reduced graphene oxide [9], polyaniline (PANI) [10], MoS_2 [3], Ti_3SiC_2 [11], and carbon nanotubes (CNTs)/multi-walled CNTs [12, 13]), and changing H_a and M_s to get desiring f_r by using cationic substitution [1, 2, 14-16]. In order to improve the microwave absorption properties of BaM, we combined the second and third approaches by substituting La to Ba site of BaM and composites with PANI, respectively.

In order to fabricate composites, we firstly prepared $Ba_{1-x}La_xFe_{12}O_{19}$ compounds with x = 0–0.5. Then, the compounds were carefully mixed with PANI to get the composites. Finally, we mixed the composites with a binder, epoxy, to prepare toroidal devices. Magnetic loss which comes from magnetic properties of composites play an important role to the microwave absorption properties. While, the drying could lead to changes of magnetic properties which were motivated us to carry out this work. In this work, we report the effects of drying on magnetic properties of composites of $Ba_{1-x}La_xFe_{12}O_{19}$/polyaniline which have divided into two batches: the first batch was as-prepared composites (named as un-dried composites) and the second batch was dried at 170°C for 30 min (named as dried composites)

2. Experimental details

La doping $BaFe_{12}O_{19}$ ($Ba_{1-x}La_xFe_{12}O_{19}$, La-BaM, x = 0–0.5) compounds were prepared by a co-precipitation method followed by heat treatment at 900°C for 3 h in a box furnace. High-purity chemicals of $Ba(NO_3)_2$, La_2O_3, and $Fe(NO_3)_3{\cdot}9H_2O$ (purchased from Sigma-Aldrich) were used as precursors. The detailed preparation process was reported in Ref. [17]. PANI was prepared from a mono-aniline solution using the polymerization method which was presented in Ref. [18]. In order to prepare the composites, La-BaM samples were mixed with PANI by the weight ratio of sample and PANI being La-BaM/PANI = 9/1. After that, the composite of La-BaM/PANI was mixed with 15 wt% epoxy. The composites

were divided into two batches: one batch was dried in a dryer at 170°C for 30 min which named as dried-composites; the other one was kept as-prepared and named as un-dried composites. Crystal structure of composites was studied by XRD (Rigaku, Miniflex model) working with a Cu-K_α radiation source (λ = 1.54056 Å). Magnetic properties of the composites were studied by using the vibrating sample magnetometer (VSM, LakeShore, model 7404) with the applied field can be varied in the range of 0–10 kOe.

3. Results and Discussion

XRD patterns of dried-composites at room temperature were presented in **Fig. 1**. PANI was crystallized in a bulk-type sample with some peaks in the range of 20–28° [19]. Meanwhile, $Ba_{1-x}La_xFe_{12}O_{19}$ samples were crystallized into the M-type hexagonal structure which belongs to the $P6_3/mmc$ space group. Because of the very low-intensity PANI peaks, there was almost no trace of PANI in the XRD patterns of $Ba_{1-x}La_xFe_{12}O_{19}$/polyaniline composites. Compared to the standard pattern of BaM hexaferrites, our composites showed some peaks of secondary phase which belonged to α-Fe_2O_3. The percentage of impurity phase increased with respect to the La doping concentration from 3.76% for x = 0 to 37.21% for x = 0.5. We also calculated lattice parameters, a and c, and volume cell, V, of the dried-composites for M-type hexaferrite phase. Both of the a and c decreased when La doping concentration increased: a decreased from 5.893 Å for x = 0 to 5.889 Å for x = 0.5; while c decreased from 23.218 Å for x = 0 to 23.114 Å for x = 0.5. Therefore, V consequently decreased from 698.369 $Å^3$ to 694.988 $Å^3$ when x increased from 0 to 0.5. The variations of a, c, and V mainly depended on the La-substitution due to low intensity of polyaniline XRD pattern peaks. The decreasing of a and c could be attributed to the substitution of a small ion (r_{La}^{3+} = 1.172 Å) for a larger ion (r_{Ba}^{2+} = 1.49 Å) [20]. The decreasing of a and c also proved that La was not replaced for Fe in $BaFe_{12}O_{19}$ hexaferrites. If so, a and c would be increased with respect to the increasing of La doping concentration because ionic radii of Fe^{3+} (r_{Fe}^{3+} = 0.785 Å) is smaller the one of La^{3+} (r_{La}^{3+} = 1.172 Å) [20]. We also found similar results in the studies of La doping BaM M-type [21, 22], La doping $SrCo_2W$ W-type [23], and La doped $BaCo_2Z$ Z-type [17] hexaferrites. The increase of secondary phase of α-Fe_2O_3 could be attributed to the generation of Fe^{2+} to keep the charge balance basing on equation $Ba^{2+} + Fe^{3+} \rightarrow La^{3+} + Fe^{2+}$ [17]. This equation meant that the more La^{3+} was introduced to the BaM, the more Fe^{2+} was generated in the BaM. The same phenomenon could be found in the work of P. Mariño-Castellanos *et. al.* with La-doping concentration up to 60% [22].

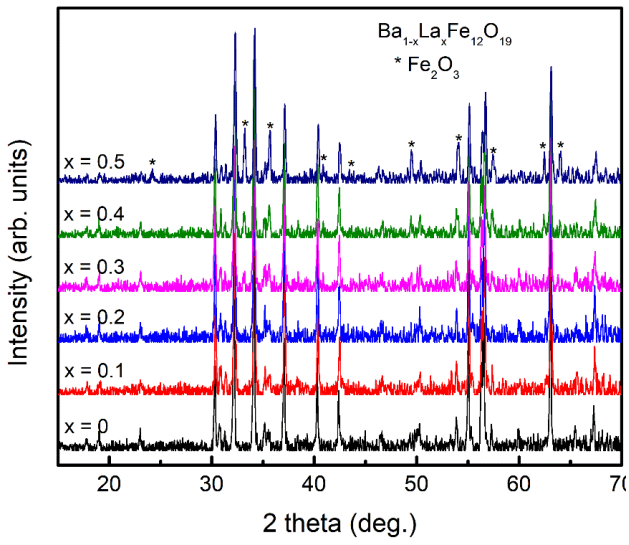

Figure 1. XRD patterns of $Ba_{1-x}La_xFe_{12}O_{19}$/polyaniline composites. The asterisks show the secondary phase of α-Fe_2O_3.

Figure 2 shows the all room-temperature $M(H)$ hysteresis loops of $Ba_{1-x}La_xFe_{12}O_{19}$/polyaniline composites. The undried composites were represented in solid-

symbol-loops and the dried composites were plotted in opened-symbol loops. In order to have a visual look, we plotted the undried and dried composites in separate figures for each sample. Obviously, all the $M(H)$ loops of our samples have a shape similar to that of other M-type ferro/ferrimagnets [14, 16, 24-26]. Values of coercivity (H_c), remanent magnetization (M_r), and M_s of all undried composites were higher than that of dried ones. Compared to the shape of loops between undried- and dried-composites, six plots in Fig. 2 could be divided into two groups. The first group included x = 0.1 (Fig. 2(b)), x = 0.3 (Fig. 2(d)), and x = 0.5 (Fig. 2(f)) which showed similar shapes between un-dried and dried composites. The second group included x = 0 (Fig. 2(a)), x = 0.2 (Fig. 2(c)), and x = 0.4 (Fig. 2(e)) which have bent and shrunk in the center parts of the loops. The values of H_c and M_r could be determined from intercepts of the loops with x- and y-axes, respectively. The values of H_c and M_r have been listed in Table 1 and Table 2.

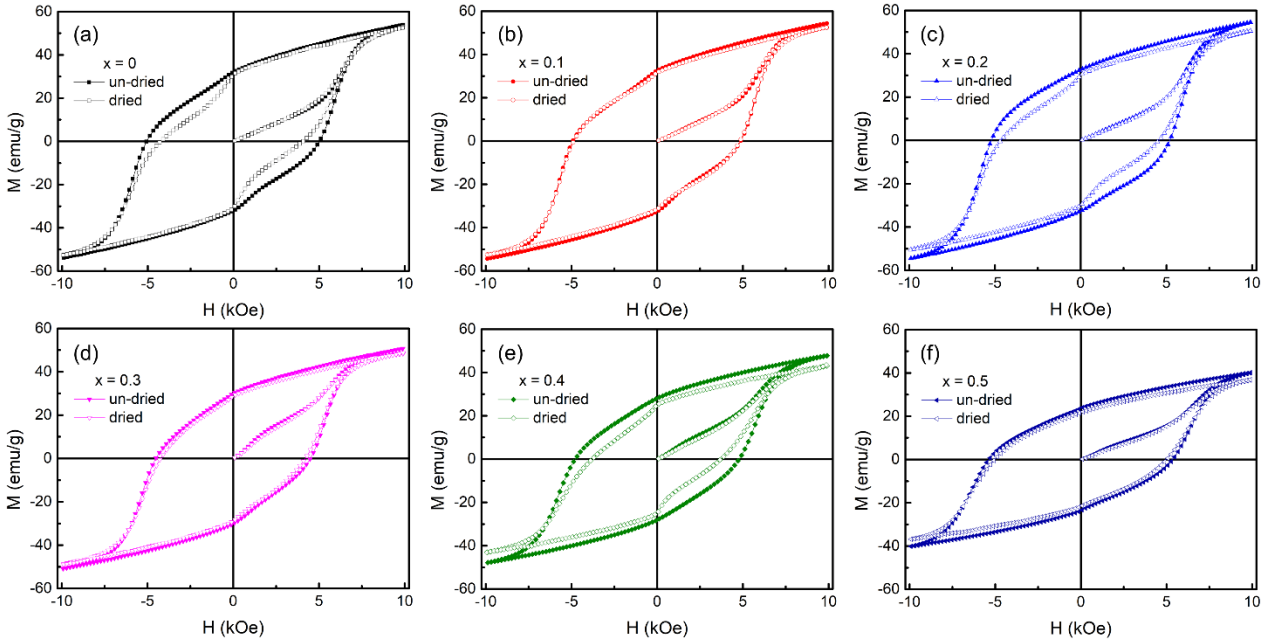

Figure 2. $M(H)$ loops for undried (solid-symbol loops) and dried (opened-symbol loops) composites of $Ba_{1-x}La_xFe_{12}O_{19}$/polyaniline with (a) x = 0, (b) x = 0.1, (c) x = 0.2, (d) x = 0.3, (e) x = 0.4, and (f) x = 0.5, respectively.

Table 1. Experimental values obtained from analyzing $M(H)$ hysteresis loops for undried composites of $Ba_{1-x}La_xFe_{12}O_{19}$/polyaniline at room temperature.

Sample (undried)	H_c (kOe)	M_r (emu/g)	M_s (emu/g)	M_r/M_s	b (10^6 Oe^2)	H_a (kOe)	K_1 (10^5 erg/cm^3)
x = 0	5.06	32.04	58.35	0.55	8.175	11.073	3.231
x = 0.1	4.91	32.52	58.86	0.55	8.019	10.967	3.228
x = 0.2	5.20	32.61	59.04	0.55	8.096	11.020	3.253
x = 0.3	4.52	29.99	54.83	0.55	7.970	10.934	2.998
x = 0.4	4.78	28.08	51.78	0.54	8.092	11.017	2.852
x = 0.5	5.37	23.72	43.53	0.54	8.293	11.153	2.428

In order to compare the H_c tendency of undried and dried composites, we plotted H_c curves as a function of La-doping concentration, as shown in Fig. 3. Obviously, H_c values of the undried composites higher than that of dried ones for all doping concentration.

In detailed, the H_c values for undried composites decreased for first doping (x = 0.1), then increased for x = 0.2, then decreased to lowest value with x = 0.3, and rose up for x = 0.4 and reached highest value for x = 0.5. The case of H_c values for dried composites were a bit simple: H_c increased for x = 0.1, then decreased for higher doping (x = 0.2–0.4), then increased for x = 0.5 composites. The lowest and highest values of H_c for dried composites were found for x = 0.4 and 0.5, respectively. The variation of H_c could be partly attributed to the present of α-Fe_2O_3 and spin canting.

In contrary to H_c, tendency of M_r values were simple (shown by red curves in Fig. 4). For undried composites, the M_r slightly increased from 32.04 emu/g for x = 0, to 32.52 emu/g for x = 0.1, to 32.61 emu/g for x = 0.2 then decreased for higher doping concentration to lowest value as M_r = 23.72 emu/g for x = 0.5. In the case of dried composites, the M_r increased from 30.63 emu/g for x = 0 to 31.47 emu/g for x = 0.1, then decreased for higher doping concentration down to M_r = 21.69 emu/g for x = 0.5. Compared between undoped and doped composites, drying reduced the M_r values with the reduction in the range of 3–11%.

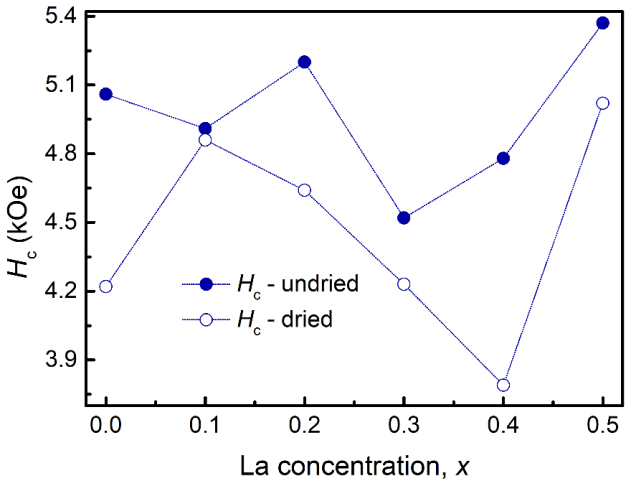

Figure 3. H_c curves as a function of La-doping concentration for undried (solid-symbol curve) and dried (opened-symbol curve) composites of $Ba_{1-x}La_xFe_{12}O_{19}$/polyaniline.

Table 2. Experimental values obtained from analyzing $M(H)$ hysteresis loops for dried composites of $Ba_{1-x}La_xFe_{12}O_{19}$/polyaniline at room temperature.

Sample (dried)	H_c (kOe)	M_r (emu/g)	M_s (emu/g)	M_r/M_s	b (10^6 Oe^2)	H_a (kOe)	K_1 (10^5 erg/cm^3)
x = 0	4.22	30.63	57.13	0.54	8.209	11.097	3.170
x = 0.1	4.86	31.47	56.82	0.55	7.955	10.924	3.103
x = 0.2	4.64	29.92	54.74	0.55	8.001	10.955	2.999
x = 0.3	4.23	28.74	52.45	0.55	7.741	10.775	2.826
x = 0.4	3.79	24.91	46.49	0.54	7.980	10.941	2.543
x = 0.5	5.03	21.69	39.77	0.55	7.996	10.952	2.178

From Fig. 2, we could observe that the hysteresis loops were not saturated in the applied magnetic field range of 0–10 kOe. Therefore, the M_s could be obtained from the hysteresis loop by employing the "Law of approach to saturation (LAS)" method. The LAS is defined as [27]:

$$M = M_s\left(1 - \frac{a'}{H} - \frac{b}{H^2}\right) + \chi H, \qquad (1)$$

where a' is inhomogeneities (approximately equal to zero) and b is magnetocrystalline anisotropy. The second term of χH is the high-field differential susceptibility related to the spontaneous magnetization of magnetic domains and active in high temperature analysis. Equation (1) could be shortened to the following equation:

$$M = M_s\left(1 - \frac{b}{H^2}\right), \quad (2)$$

In this work, Eq. (2) was used to fit the $M(H)$ data at high field of H = 7–10 kOe. The values of M_s were plotted in Fig. 4 by black curves. For undried composites, M_s slightly increased from 58.35 emu/g for x = 0 to 58.86 emu/g for x = 0.1, to 59.04 emu/g for x = 0.2, then decreased for higher doping concentration. While, the M_s values of dried composites decreased when La concentration increased. Similar to M_r values, the M_s values of dried composites were lower than undried composites with reduction of 2–10 %. The decreasing of M_r and M_s was caused by the replacement of Ba^{2+} by La^{3+}, as well as by the presence of the secondary phase. Due to the substitution of Ba^{2+} by La^{3+}, the ionic state of Fe reduced from Fe^{3+} to Fe^{2+} which might decrease the strength of the Fe^{3+}–O–Fe^{3+} double-exchange interactions. In addition, the weakening of magnetization could be attributed to spin canting [15, 28]. On the other hand, the secondary phase of hematite (α-Fe_2O_3) is antiferromagnetic which could also be a contributor to the reduction of M_s and M_r values. We also calculated the squareness ratio M_r/M_s of undried and dried composites (listed in Table 1 and Table 2). Considering the M_r/M_s ratio, the following phenomena was determined: (i) M_r/M_s < 0.5: there is a dominance of the magnetostatic interaction between particles; (ii) M_r/M_s = 0.5: there is a dominance of randomly oriented non-interacting particles under coherent rotation; and (iii) 0.5 < M_r/M_s < 1: exchange coupling between particles takes place [29]. In our work, M_r/M_s values were in the range of 0.54–0.55, proving the exchange coupling between particles existed in undried and dried composites of $Ba_{1-x}La_xFe_{12}O_{19}$/polyaniline.

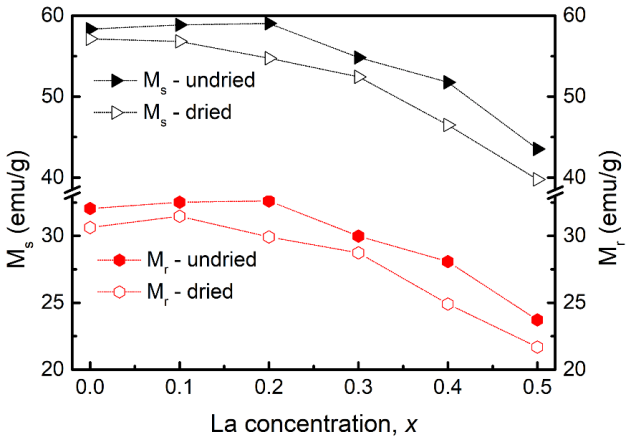

Figure 4. M_s and M_r curves as a function of La-doping concentration for undried (solid-symbol curves) and dried (opened-symbol curves) composites of $Ba_{1-x}La_xFe_{12}O_{19}$/polyaniline.

By using LAS, we also determined magnetocrystalline anisotropy, b, from the slope of fitting line of magnetization where slope is a product of b and M_s. The b values of undried and dried composites were shown in the *top* plot of Fig. 5. The curves of b have similar tendency to the curves of H_c for undried composites. Compare the b curves between undried and dried composites, the b values of undried composites were higher than the dried ones except x = 0 composite. The K_1 values of undried and dried composites also calculated through the following expression:

$$b = \frac{H_a^2}{15} = \frac{4K_1^2}{15M_s^2}, \quad (3)$$

With b and M_s obtained above, we have calculated the values of H_a and K_1, listed in Table 1 and Table 2. From Eq. (3), we could clearly observe that H_a is directly proportion to b. Therefore, the H_a has the variation tendencies similar to that of b, as shown in the *bottom* plot of Fig. 5.

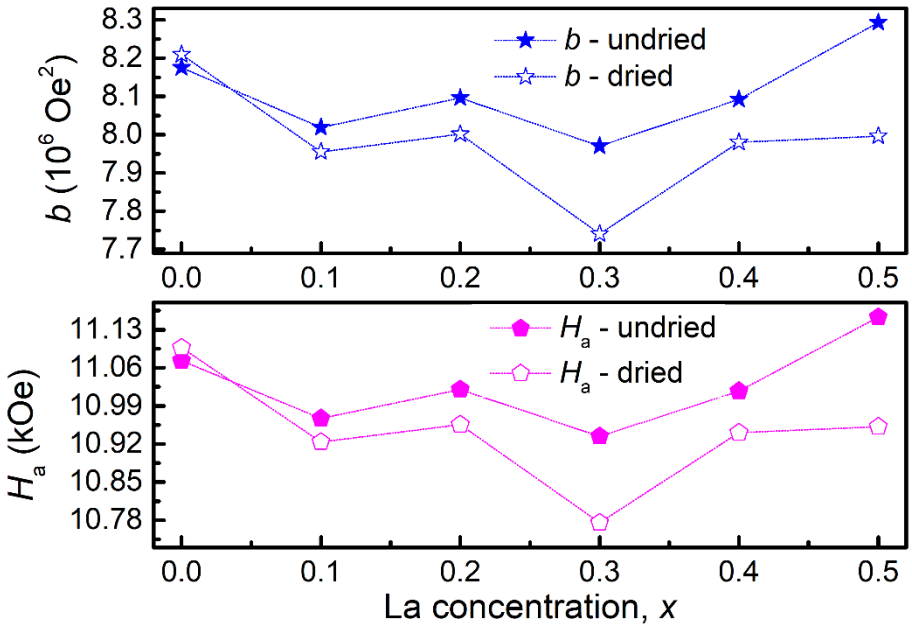

Figure 5. *(top)* Magnetocrystalline anisotropy, *b*, and *(bottom)* magnetocrystalline anisotropy field, H_a, curves as a function of La-doping concentration for undried (solid-symbol curves) and dried (opened-symbol curves) composites of $Ba_{1-x}La_xFe_{12}O_{19}$/polyaniline.

While, the K_1 values which calculated through Eq. (3) showed the similar tendencies the that of M_s curves, as shown in Fig. 6. Overall, all the magnetic parameters such as M_s, M_r, H_c, *b*, H_a, and K_1 of the dried composites were smaller than the undried ones. This phenomenon could be attributed to the changes in the density of composites after drying.

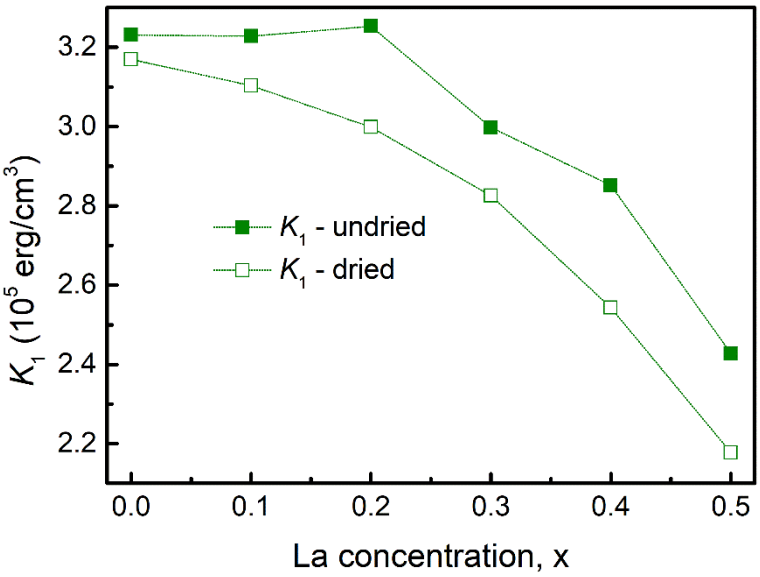

Figure 6. Magnetocrystalline anisotropy constant, K_1, curves as a function of La-doping concentration for undried (solid-symbol curve) and dried (opened-symbol curve) composites of $Ba_{1-x}La_xFe_{12}O_{19}$/polyaniline.

4. Conclusion

The undried and dried composites of $Ba_{1-x}La_xFe_{12}O_{19}$/polyaniline were successfully prepared. The structural properties of dried composites studied by XRD which showed the presence of impurity phase of α-Fe_2O_3. The phase percentage of α-Fe_2O_3 increased with respect to the increase of La doping concentration. Magnetic properties of $Ba_{1-x}La_xFe_{12}O_{19}$/polyaniline composites were

strongly depending on the drying. The drying at 170°C led to the decreasing in the values of saturation magnetization, remanent magnetization, coercivity, magnetocrystalline anisotropy, magnetocrystalline anisotropy constant, and magnetocrystalline anisotropy field. The changing in the magnetic parameters would affect the microwave absorption properties of composites. We hope this paper could contribute a sight about effects of drying on magnetic properties and researchers could select whether using drying or not and which drying temperature could be good for magnetic and microwave absorption properties of hexaferrite/polyaniline composites.

References

[1] M.A. Almessiere, Y. Slimani, S. Guner, S. Aldakhil, A.D. Korkmaz, M. Sertkol, H. Gungunes, G. Yasin, A. Baykal, 2020. Ultrasonic synthesis, magnetic and optical characterization of Tm^{3+} and Tb^{3+} ions co-doped barium nanohexaferrites. J. Solid State Chem. 286, 121310.

[2] W. Widanarto, F. Amirudin, S.K. Ghoshal, M. Effendi, W.T. Cahyanto, 2017. Structural and magnetic properties of La^{3+} substituted barium−natural nanoferrites as microwave absorber in X-band. J. Magn. Magn. Mater. 426, 483-486.

[3] M. Wang, Y. Lin, H. Yang, Y. Qiu, S. Wang, 2020. A novel plate-like $BaFe_{12}O_{19}$@MoS_2 core-shell structure composite with excellent microwave absorbing properties. J. Alloys .Compd. 817, 153265.

[4] A.R. Kagdi, N.P. Solanki, F.E. Carvalho, S.S. Meena, P. Bhatt, R.C. Pullar, R.B. Jotania, 2018. Influence of Mg substitution on structural, magnetic and dielectric properties of X-type bariumzinc hexaferrites $Ba_2Zn_{2-x}Mg_xFe_{28}O_{46}$. J. Alloys .Compd. 741, 377-391.

[5] Y. Lin, Y. Liu, J. Dai, L. Wang, H. Yang, 2018. Synthesis and microwave absorption properties of plate-like $BaFe_{12}O_{19}$@Fe_3O_4 core-shell composite. J. Alloys .Compd. 739, 202-210.

[6] C. Pahwa, S.B. Narang, P. Sharma, 2019. Interfacial exchange coupling driven magnetic and microwave properties of $BaFe_{12}O_{19}/Ni_{0.5}Zn_{0.5}Fe_2O_4$ nanocomposites. J. Magn. Magn. Mater. 484, 61-66.

[7] C. Pahwa, S. Mahadevan, S.B. Narang, P. Sharma, 2017. Structural, magnetic and microwave properties of exchange coupled and non-exchange coupled $BaFe_{12}O_{19}/NiFe_2O_4$ nanocomposites. J. Alloys .Compd. 725, 1175-1181.

[8] Y. Liu, Y. Lin, H. Yang, 2019. Facile fabrication for core-shell $BaFe_{12}O_{19}$@C composites with excellent microwave absorption properties. J. Alloys .Compd. 805, 130-137.

[9] S. Goel, A. Garg, R.K. Gupta, A. Dubey, N.E. Prasad, S. Tyagi, 2020. Development of RGO/$BaFe_{12}O_{19}$-based composite medium for improved microwave absorption applications. Appl. Phy. A 126, 436.

[10] M. Wang, Y. Lin, Y. Liu, H. Yang, 2019. Core–shell structure $BaFe_{12}O_{19}$@PANI composites with thin matching thickness and effective microwave absorption properties. J. Mater. Sci.: Mater. Electron. 30, 14344-14354.

[11] Y. Liu, X. Su, F. Luo, J. Xu, J. Wang, X. He, Y. Qu, 2019. Enhanced Electromagnetic and Microwave Absorption Properties of Hybrid Ti_3SiC_2/$BaFe_{12}O_{19}$ Powders. J. Electron. Mater. 48, 2364-2372.

[12] A. Afzali, V. Mottaghitalab, S.S. Seyyed Afghahi, M. Jafarian, Y. Atassi, 2017. Electromagnetic properties of absorber fabric coated with $BaFe_{12}O_{19}$/MWCNTs/PANi nanocomposite in X and Ku bands frequency. J. Magn. Magn. Mater. 442, 224-230.

[13] T. Zhao, X. Ji, W. Jin, S. Guo, H. Zhao, W. Yang, X. Wang, C. Xiong, A. Dang, H. Li, T. Li, S. Shang, Z. Zhou, 2017. Electromagnetic wave absorbing properties of aligned amorphous carbon nanotube/$BaFe_{12}O_{19}$ nanorod composite. J. Alloys .Compd. 703, 424-430.

[14] M. Cernea, S.-G. Sandu, C. Galassi, R. Radu, V. Kuncser, 2013. Magnetic properties of $Ba_xSr_{1-x}Fe_{12}O_{19}$ (x=0.05–0.35) ferrites prepared by different methods. J. Alloys .Compd. 561, 121-128.

[15] H. Sözeri, İ. Küçük, H. Özkan, 2011. Improvement in magnetic properties of La substituted $BaFe_{12}O_{19}$ particles prepared with an unusually low Fe/Ba molar ratio. J. Magn. Magn. Mater. 323, 1799-1804.

[16] P. Sharma, R.A. Rocha, S.N. Medeiros, B. Hallouche, A. Paesano, 2007. Structural and magnetic studies on mechanosynthesized $BaFe_{12-x}Mn_xO_{19}$. J. Magn. Magn. Mater. 316, 29-33.

[17] N. Tran, T.L. Phan, N.T. Dang, D.S. Yang, B.W. Lee, 2019. Crystalline and electronic structure and magnetic properties of La-doped $Ba_3Co_2Fe_{24}O_{41}$ hexaferrites. J. Phys. Chem. Solids 131, 55-61.

[18] A. Mostafaei, A. Zolriasatein, 2012. Synthesis and characterization of conducting polyaniline nanocomposites containing ZnO nanorods. Prog. Nat. Sci. 22, 273-280.

[19] A. Mostafaei, A. Zolriasatein, 2012. Synthesis and characterization of conducting polyaniline nanocomposites containing ZnO nanorods. Pro. Na. Sci-Mater. 22, 273-280.

[20] R.D. Shannon, 1976. Revised effective ionic radii and systematic studies of interatomic distances in halides and chalcogenides. Acta Crystallogr. Sect. A 32, 751-767.

[21] S. Kumar, M. Kumar Manglam, S. Supriya, H. Kumar Satyapal, R. Kumar Singh, M. Kar, 2019. Lattice strain mediated dielectric and magnetic properties in La doped barium hexaferrite. J. Magn. Magn. Mater. 473, 312-319.

[22] P. Mariño-Castellanos, F. Guerrero, Y. Romaguera-Barcelay, E. Goveia-Alcaide, E.A. Cotta, Y. Leyet, J. Anglada-Riveira, E. Padrón-Hernández, R. Peña-Garcia, 2020. Effect of La^{3+} cation solubility on the structural, magnetic and electrical properties of barium hexaferrite. Ceram. Int. 47 (2021) 8236-8247.

[23] X. Niu, Y. Liu, M. Li, B. Wu, H. Li, 2017. The Study of Microstructure and Magnetic Properties of La^{3+} doped W-Type Hexagonal Ferrites $Sr_{1-x}La_xCo_2Fe_{16}O_{27}$. J. Electron. Mater. 46, 4299-4303.

[24] N. Tran, H.S. Kim, T.L. Phan, D.S. Yang, B.W. Lee, 2018. Electronic structure and magnetic properties of $Ba_{1-x}Sr_xCoFe_{11}O_{19}$ hexaferrites. Ceram. Int. 44, 12132-12136.

[25] F.N. Tenorio-González, A.M. Bolarín-Miró, F. Sánchez-De Jesús, P. Vera-Serna, N. Menéndez-González, J. Sánchez-Marcos, 2017. Crystal structure and magnetic properties of high Mn-doped strontium hexaferrite. J. Alloys .Compd. 695, 2083-2090.

[26] E. Kiani, A.S.H. Rozatian, M.H. Yousefi, 2014. Structural, magnetic and microwave absorption properties of $SrFe_{12-2x}(Mn_{0.5}Cd_{0.5}Zr)_xO_{19}$ ferrite. J. Magn. Magn. Mater. 361, 25-29.

[27] A.M. Alsmadi, I. Bsoul, S.H. Mahmood, G. Alnawashi, K. Prokeš, K. Siemensmeyer, B. Klemke, H. Nakotte, 2013. Magnetic study of M-type doped barium hexaferrite nanocrystalline particles. J. Appl. Phys. 114, 243910.

[28] D. Bueno-Báques, E. Padrón Hernandez, J. Matutes-Aquino, S.M. Rezende, D.R. Cornejo, 2004. Study of magnetization reversal in hybrid magnets. J. Alloys .Compd. 369, 158-161.

[29] J.F. Wang, C.B. Ponton, R. Grössinger, I.R. Harris, 2004. A study of La-substituted strontium hexaferrite by hydrothermal synthesis. J. Alloys .Compd. 369, 170-177.